Article:
DiCorato, AE, Asenath-Smith, E, Kulak, AN orcid.org/0000-0002-2798-9301 et al. (2 more authors) (2016) Cooperative Effects of Confinement and Surface Functionalization Enable the Formation of Au/Cu2O Metal-Semiconductor Heterostructures. Crystal Growth and Design, 16 (12). pp. 6685-7324. ISSN 1528-7483

https://doi.org/10.1021/acs.cgd.6b00913

Title:
Cooperative Effects of Confinement and Surface Functionalization Enable the Formation of Au/Cu_2O Metal-Semiconductor Heterostructures

Authors:
Allessandra E. DiCorato[1,a], Emily Asenath-Smith[2,b,*], Alex N. Kulak[3], Fiona C. Meldrum[3], and Lara A. Estroff[2,4,*]

[1] Department of Chemistry and Chemical Biology, Baker Laboratory, Cornell University, Ithaca, NY 14853, USA

[2] Department of Materials Science and Engineering, Bard Hall, Cornell University, Ithaca, NY 14853, USA

[3] School of Chemistry, University of Leeds, Leeds LS2 9JT, UK

[4] Kavli Institute for Nanoscale Science, Physical Sciences Building, Cornell University, Ithaca, NY 14853, USA

*co-corresponding authors, E-mail: lae37@cornell.edu; emily.asenath-smith@usace.army.mil

a) current address: Department of Materials Science and Engineering, Northwestern University, Evanston, IL 60208

b) current address: US Army Engineer Research and Development Center, Hanover, NH 03755

Abstract: A promising approach to obtaining multi-functional materials with tunable properties is the incorporation of second phase constituents (e.g., particles, fibers) within inorganic crystals. To date, however, the specific chemical and physical controls over incorporation are only known for a few select systems. In this study, a simple wedge is used as a confining structure to systematically control the chemical and physical aspects of the crystallization microenvironment to promote the interaction between copper (I) oxide (Cu_2O) crystals and alkanethiol-functionalized gold nanoparticles (Au np), producing a metal-semiconductor composite. Physically, the confining wedge geometry provides (vapor) diffusion-limited growth conditions. Chemically functionalizing both the Au np surfaces and the glass slides that form the wedge promotes the interaction of Au np with the growing Cu_2O crystals. The physical confinement of the wedge structure, as well as optimization of its surface chemistry are required to achieve this interaction. These findings demonstrate that Au/Cu_2O can be used as a model system to inform the synthesis of other metal-semiconductor heterostructures.

Introduction

Combining metallic and semiconductor nanomaterials into heterostructures has recently gained attention as a route to functional materials for many optoelectronic applications.[1-4] Nanoscale constituents such as gold nanoparticles (Au nps) have been paired with transition metal oxides to extend the wavelengths of absorption in photovoltaic materials,[5,6] to tune photocatalytic properties,[7] and to improve sensor response.[8-10] The synthetic approaches used to facilitate the metal-semiconductor interaction have varied widely from chemical functionalization of substrates[11] to post-synthesis decoration on the surface of crystals.[7] In related work, advances have been made in synthetic methods to entrap polymeric particles and fibers within ionic single crystals.[12-15] In the current work, we combine physical and chemical strategies to promote the interaction of Au nps with Cu_2O crystals during growth, and in this manner achieve surface decoration of single crystals with well-defined morphologies.

Chemical functionality and physical confinement have both been used as strategies for promoting the incorporation of second phase particles within crystals. In bulk solutions, chemical approaches to promote the incorporation of particles within inorganic crystals largely involve carefully tuned surface chemistry of second phase particles.[16-18] For example, carboxylic acid surface functionality has been key to the incorporation of polystyrene colloids into numerous inorganic crystals, including calcite,[19] zincite,[20] and cuprite.[19] In these examples, the crystals were on the order of 10 micrometers, while the colloids were hundreds of nanometers in diameter. More sophisticated surface chemistries have been needed to apply these strategies to the incorporation of nanoscale (1-10 nm) constituents. Diblock copolymers with dual functionality and spatially separated charges have been used to regulate the nanoparticle/crystal interaction, and gold[17] and magnetite[16] nanoparticles have been occluded within calcite crystals using this strategy. One important aspect of these successes was the large relative fraction of the polymeric constituents encompassing the particles; the diameter of the polymer coating was on the order of the particle diameter.[16] From studies with diblock

copolymer micelles[12,21] it is clear that the compliance of the nanoscale constituent also plays a role in its successful encapsulation.

As a physical aspect of the crystallization microenvironment, confined volumes have been used to alter nucleation times,[22] to limit the diffusion of reagents,[23] and to limit the diffusion of larger objects (nanoparticles, etc.).[24] Many synthetic models such as track-etched membranes,[25,26] crossed cylinders,[27,28] nanoporous substrates,[29,30] vesicles,[31,32] Vycor glasses,[33] and microfluidic devices[34] have been used to probe the physical effects of confinement on crystallization.[35,36] Notably, single crystal composites, in which calcite single crystals are forced to grow within a colloidal array of polystyrene spheres, have been achieved within the confines of a simple wedge structure.[18] In this system, it was found that the physical confinement of the colloidal crystal within the wedge structure favored occlusion of the polystyrene within calcite crystals during growth. Significantly, chemical functionalization of the colloidal surfaces was not required for complete entrapment of the polystyrene colloids. While this strategy demonstrated a purely physical means to form single crystal composites, the length scales of these particles and crystals are too large for many optoelectronic applications, in which the electron mean free path (~10 nm) is a critical design criterion.[37] Thus, the question of how to translate this method to encapsulate nanoscale objects still remains. Methods to employ these approaches in the synthesis of multi-functional semiconducting crystals are also needed.

In the family of semi-conducting transition metal oxides there are a few select reports of single crystal composites of Cu_2O with occluded polystyrene colloids.[19,38,39] Such interactions have been achieved by carefully tuning the surface chemistry of the colloids[19] or by application of an external potential.[38,39] While chemical functionalization of gold nanoparticle surfaces is common,[17,40-42] it has rarely been used as an approach to encapsulate Au np within inorganic crystals.[17] Furthermore, the use of physically confined volumes is known to facilitate the incorporation of particles within crystals,[18] but has yet to be applied to a metal-semiconductor pair. In our current work, we focus on the interplay between chemical functionalization and

physical confinement to facilitate the interaction of Cu_2O crystals with Au nps during crystallization (Scheme 1).

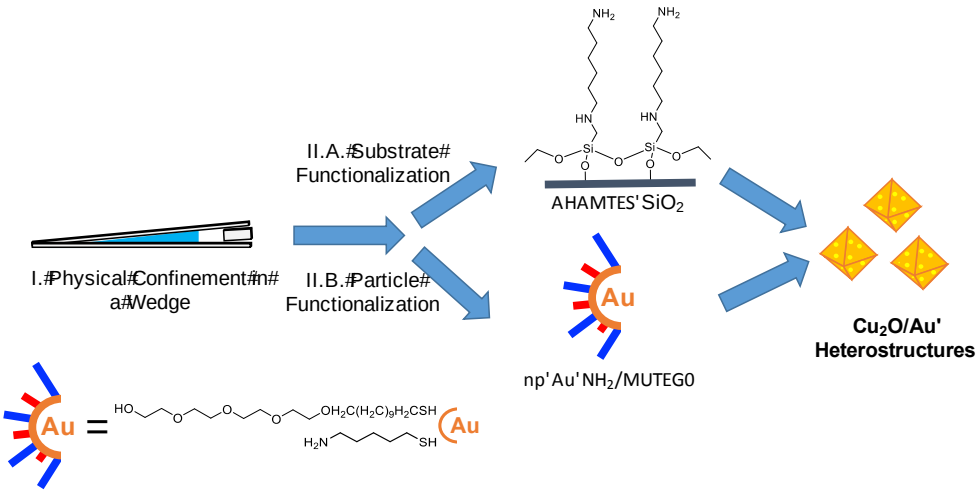

Scheme 1. Strategy for introducing physical and chemical effects into the crystallization microenvironment. I. Crystallization in confinement first allowed for physical manipulation of the system. II. Subsequent chemical manipulation, by functionalizing both the glass substrate (II.A) and the gold nanoparticles (II.B), enabled the formation of Cu_2O/Au heterostructures.

Experimental Section

Materials

Hydrogen tetrachloroaurate (99.99%, Sigma-Aldrich), sodium citrate tribasic dihydrate (≥98%, Sigma-Aldrich), (±)-α-lipoic acid (≥99%, Sigma-Aldrich), 6-amino-1-hexanethiol hydrochloride (Sigma-Aldrich), 6-mercaptohexanoic acid (90%, Sigma-Aldrich), (1-mercaptoundec-11-yl)tetra(ethylene glycol) (95%, Sigma-Aldrich), copper (II) sulfate pentahydrate (98%, Sigma-Aldrich), sodium hydroxide pellets (99.2%, Fisher), hydrazine hydrate (78-82%, Sigma-Aldrich), N-(6-aminohexyl)aminomethyltriethoxysilane (95%, Gelest), molecular sieves UOP Type 3A (Fluka Analytical), and ethanol (100%, Pharmaco-Aaper) were used as received.

Nanoparticle Preparation

Synthesis. Citrate-stabilized gold nanoparticles ("np-Au-cit") were prepared using the Turkevitch method.[43] Briefly, 50 mL of $3.55x10^{-4}$ M $HAuCl_4$ (in deionized water) was brought to a rolling boil while stirring under reflux. Subsequently, 2 mL 1 w/v% sodium citrate were added to the boiling solution. The color of the solution was observed to change from pale yellow to purple to wine red over the course of five minutes. Subsequently, the solution was refluxed for an additional 20 minutes and allowed to cool before proceeding with surface functionalization via ligand exchange (described below). Particles at this stage were stored in the dark and used within 1 month. Gold nanoparticles were characterized using dynamic light scattering (DLS) and zeta-potential to determine size and surface charge, respectively (Zetasizer Nano ZS, Malvern Instruments Ltd., Worcestershire, UK). Nanoparticle size and crystallinity (Figure S1) were confirmed with transmission electron microscopy (Tecnai T12, FEI, USA). Approximate concentration of the functionalized nanoparticle solution was determined using UV/Vis spectroscopy (Spectramax Plus384 Absorbance Microplate Reader, Molecular Devices, USA).[44]

Lipoic Acid Functionalization. Citrate-stabilized gold nanoparticles were functionalized with carboxylate and amine groups using a modified version of the procedure reported by Ivanov et al. wherein the citrate surface moieties are initially ligand exchanged to lipoic acid.[40] Briefly, 0.6 mL 4 mM lipoic acid in ethanol was added to 6 mL citrate-stabilized gold nanoparticles while stirring at 350 RPM. After stirring overnight at room temperature, the particles were centrifuged at 14000 RPM for 20 minutes and re-dispersed in an equal volume of water.

Ligand Exchange. 0.6 mL of 4 mM 6-amino-1-hexanethiol in ethanol was added to 6 mL of the TA-functionalized nanoparticles while stirring in a refrigerator set to 4℃. After 1 hour, 0.6 mL 1 M HCl was added to the solution. The solution was stirred overnight in the refrigerator. The following day, particles were centrifuged at 14000 RPM for 20 minutes and re-dispersed in water. Particles ("np-Au-NH_2") were stored in the dark (4 ℃) and used within one week. To

functionalize with 6-amino-1-hexanethiol hydrochloride/MUTEG ("np-Au-NH_2/MUTEG"), 0.3 mL of 4 mM (1-mercaptoundec-11-yl)tetra(ethylene glycol) in ethanol and 0.3 mL of 4 mM 6-amino-1-hexanethiol in ethanol were added sequentially. Gold nanoparticles were characterized using zeta-potential to determine surface charge (Zetasizer Nano ZS, Malvern Instruments Ltd., Worcestershire, UK). All measurements were taken with gold nanoparticles in their native solutions.

Substrate Preparation and Silanization.

Standard microscope slides were submersed in a freshly prepared piranha solution consisting of three parts H_2SO_4 and one part H_2O_2. Caution: piranha solution reacts violently with organic matter. Slides were removed from the piranha solution after one hour, rinsed several times with water, and dried for 30 minutes in an oven heated to 80℃. Deoxygenated ethanol was prepared by adding 5 g molecular sieves to 200 mL ethanol in a round bottomed flask. The ethanol was bubbled with flowing nitrogen overnight and kept sealed under nitrogen until use.

Substrates were functionalized using a modified procedure from the literature.[45] Freshly cleaned dry slides were sealed in a 50 mL centrifuge tube and degassed with flowing nitrogen. Subsequently, 45 mL deoxygenated ethanol was transferred into the tubes under nitrogen. Lastly, 450 µL N-(6-aminohexyl)aminomethyltriethoxysilane (AHAMTES) was added using a gas-tight syringe. No liquid silane was allowed to touch the samples directly. Slides were allowed to remain undisturbed in an oven heated to 80℃. After 4 hours, the slides were rinsed with ethanol (2x), water (1x), and ethanol (1x) before drying for 30 minutes in an oven heated to 80℃. Substrates were stored under vacuum and used within two days of silanization. The quality of the substrates was characterized by atomic force microscopy (Nanoscope III, Digital Instruments, Santa Barbara, USA), ellipsometry (Nanofilm EP3, Accurion, Germany), and contact angle goniometry (Model 500, Rame-Hart, Succasuna, USA).

Crystallization of Copper (I) Oxide in Wedge

A crystallization wedge (Figure 1) was designed using a modified version of that reported by Meldrum and co-workers.[18] Specifically, the wedge was constructed from two silanized slides propped open at an angle of 0.93° by placing a small piece of slide (0.1 x 0.7 x 0.7 cm) between two slides (top slide: 0.1 x 7.0 x 2.5 cm; bottom slide: 0.1 x 7.5 x 2.5 cm). The internal volume of the wedge was approximately 0.775 mL (6.2 x 2.5 cm base; 0.1 cm height). The wedge was centered over a petri dish with a diameter of 60 mm inside a custom-built double-walled reactor. Heating was accomplished by circulating water through the double-walled chamber so that an internal temperature of ~55℃ was achieved.

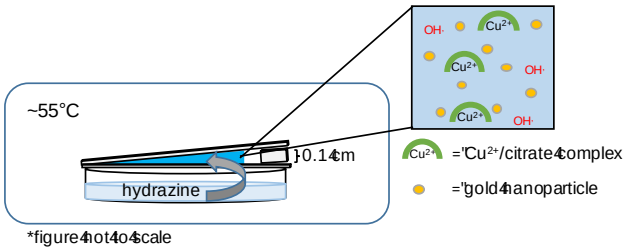

Figure 1. Side view of crystallization wedge. The crystallization solution contains copper (II) ions complexed by citrate ions, hydroxide ions, and gold nanoparticles (sulfate and sodium ions not shown). The entire set up is sealed in a heated reactor to induce crystallization via vapor diffusion of a reductant. (Schematic not to scale.)

Crystallization of Cu_2O was achieved using a modified Fehling's solution in which the reducing agent was supplied to the basic copper citrate solution by vapor diffusion of hydrazine rather than an aqueous solution of glucose.[46] To prepare the crystallization solution 0.5 mL of 0.074 M sodium citrate was first added to 0.5 mL 0.068 M $CuSO_4$ while stirring, followed by the dropwise addition of 0.75 mL of functionalized gold nanoparticles. Lastly, 0.25 mL of 0.24 M NaOH was added while stirring. Using a pipette, approximately 0.775 mL of the final solution was slowly added to the open end of the wedge allowing capillary action to draw the solution into the narrowest end of the wedge until the wedge was entirely filled with the crystallization solution. In the petri dish, 2 mL hydrazine hydrate (78%-82%) was added to 18 mL water (for a final volume of 20 mL). After sealing the vessel, the reaction was allowed to proceed for 3.5

hours. At this time, approximately two-thirds of the wedge was dry (regions A, B, Figure 2). Upon removal from the vessel, the glass slides of the wedge were thoroughly rinsed twice with water before rinsing with ethanol and allowing to air dry before storage under vacuum.

Crystallization of Copper (I) Oxide in Solution

To prepare the crystallization solution 1.5 mL of 0.074 M sodium citrate was first added to 1.5 mL 0.068 M $CuSO_4$ while stirring, followed by the dropwise addition of 2.25 mL of functionalized gold nanoparticles. Lastly, 0.75 mL of 0.24 M NaOH was added while stirring, resulting in the same concentrations of reagents as in standard experiments. A scintillation vial containing the crystallization solution was balanced over a dish of hydrazine (2 mL hydrazine hydrate (78%-82%) and 18 mL water, for a final volume of 20 mL) and placed in the sealed and heated reactor for 11 hours. Resulting crystals were allowed to cool in solution for 30 minutes before centrifuging at 14000 RPM for 3 minutes. Crystals were rinsed with water and centrifuged at 14000 RPM for 3 minutes (1x) and rinsed with ethanol and centrifuged at 14000 RPM for 3 minutes (2x).

Characterization of Cu_2O Materials

Post crystallization, the bottom slide of the wedge was prepared for SEM by coating with approximately 5-10 nm carbon. For crystals grown in solution, samples were drop cast onto silicon wafers and examined (uncoated) by SEM. All samples were examined using a field-emission scanning electron microscope (Leo1550, Zeiss Microscopy, USA) operating at 5 kV.

Crystal phase was determined by powder x-ray diffraction using a Scintag theta-theta diffractometer (XDS2000) with CuK_α radiation operating at 40 kV and 30 mA with a scan rate of 2 deg/min. The entire slide was placed on the stage for analysis.

The encapsulation of the Au np within the copper oxide crystals was studied by transmission electron microscopy operating in bright field conditions (Tecnai T12, FEI, USA; LaB_6 filament operating at 120 kV). The crystalline heterostructures were removed from the wedge surfaces with a razor and dispersed onto carbon-coated copper grids for imaging.

Results

Crystallization of Cu_2O in a Wedge. In order to grow cuprite crystals in confinement, we developed a crystallization wedge in which glass slides served both as substrates and the confining features of the crystallization setup.[18] The confined volume for the crystallization of copper oxide was constructed using glass slides in a wedge-like geometry (Fig. 1). A basic (pH 12) copper (II)/citrate solution was then loaded into the wedge by capillary action. Upon heating in a sealed chamber (~55 ℃), crystallization of Cu_2O within the wedge was induced by the vapor diffusion of hydrazine. After crystallization, the crystals grown on the bottom slide of the wedge were characterized with optical microscopy, scanning electron microscopy (SEM), and powder x-ray diffraction (pXRD).

At the macroscale, the bottom slide of the wedge had visible variations in color. Bright orange regions were observed along the edges and a black-orange area was observed towards the middle of the substrate (Fig. 2, center). Observation by SEM revealed distinct crystal morphologies associated with the different colors. Octahedra, expressing {111} planes, were located in the bright orange regions “A” (Fig. 2A), while poorly-formed aggregates were located towards the black middle of the wedge (Fig. 2B), growing sparser away from the edges of the substrate and towards the bottom (Fig. 2C). Additionally, crystals found near the closed end of the wedge had morphologies that were more variable than those of the crystals found near the open end or the edges. When the entire slide was analyzed by pXRD, only the cuprite phase was identified (Fig. S1a), suggesting that both the bright orange octahedra and the darker colored aggregates were the same phase.

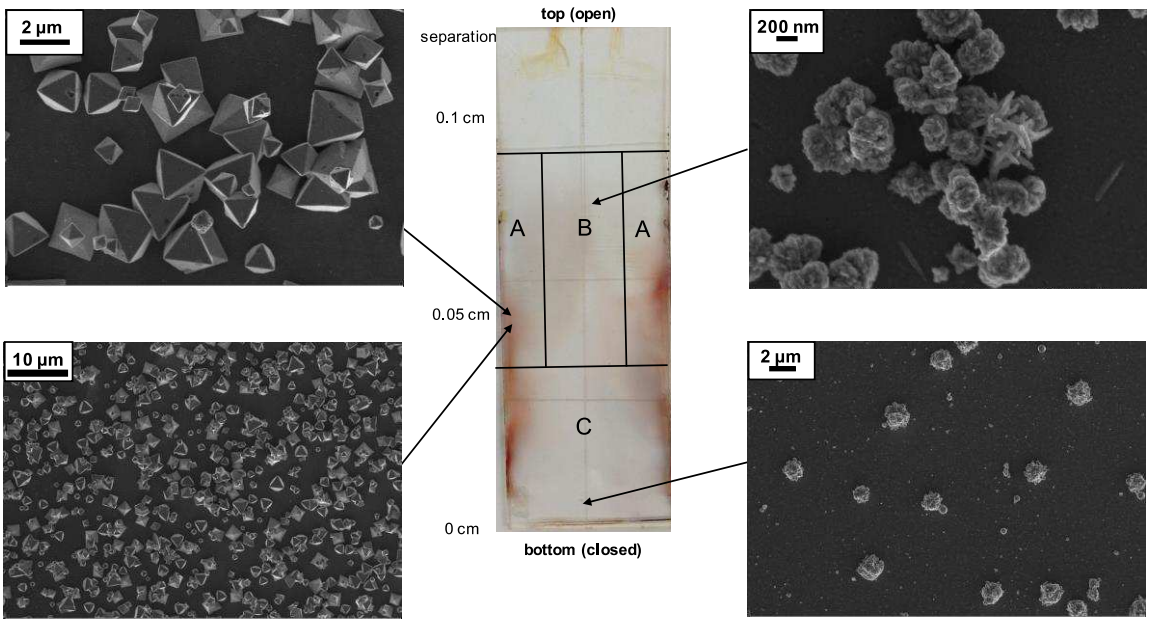

Figure 2. Images from piranha cleaned glass slide and Cu_2O crystallization. (Center) Optical image of full 2.5 x 7.5 cm slide showing orange and black coverage on the slide; crystals from all areas were confirmed to be Cu_2O with pXRD. Spacing between the top and bottom slides of the wedge indicated on the left side of the optical image. (Sides) SEM images indicating the crystal morphologies obtained at different positions of the bottom slide of the wedge. (A) Octahedral Cu_2O crystals corresponding to orange areas. (B) Poorly formed Cu_2O aggregates corresponding to black areas. (C) Sparse Cu_2O crystals of variable morphology in areas of high confinement and limited diffusion.

Chemical Functionalization of the Crystallization Microenvironment. After establishing that cuprite octahedra could successfully be grown in the confinement of the wedge geometry, we next sought to increase both the coverage of Cu_2O on the glass slides. Based upon literature reports that amine-functionalized surfaces promote the growth of Cu_2O, we functionalized the glass slides in the wedge to direct the growth of cuprite crystals on the surfaces (Scheme 1).[11,47] In order to ensure a hydrolytically-stable amine-terminated layer for the aqueous crystallizations, glass components of the wedge were functionalized with N-(6-aminohexyl)aminomethyltriethoxysilane (AHAMTES).[45] The silane layers had thicknesses of 15-20 Å and 50-60° contact angles (determined with ellipsometry and contact angle goniometry, respectively). By AFM, the silanized slides appeared homogeneous with rms roughness of less than 5 Å. Compared to unfunctionalized glass slides, the amine-functionalized wedge surfaces promoted better adhesion of the Cu_2O crystals to the substrate, qualitatively observed during post-crystallization rinsing. The distribution and morphology of the crystals within the wedge appeared unchanged on the (AHAMTES) silanized slides, as octahedra (expressing {111} planes) were maintained (data not shown).

Physical and Chemical Effects Promote the Au-Cu_2O Interaction. Having optimized the substrate-Cu_2O interaction, we next investigated the ability of physical confinement to facilitate the formation of metal-semiconductor heterostructures. Since amine functionalization promoted the adhesion of Cu_2O to the glass slides, we began our experiments with amine-functionalized gold nanoparticles. We used a thiol-based ligand exchange procedure on citrate-stabilized cores to introduce the amine functionality.[40] Monodispersed citrate-stabilized gold particles with size 17.0 +/- 1.62 nm (measured using TEM images; n=61, Fig. S2) and zeta potential -18.8 +/- 0.4 mV (Table 1) were synthesized using a modified version of the Turkevitch method[43,48] and they were subsequently functionalized with 6-amino-1-hexanethiol hydrochloride. The np-Au-NH_2 had an average zeta potential of 31.9+/-7.2 mV (Table 1).

Table 1. Gold nanoparticle characterization.[1]

Functionalization	Zeta potential (mV)	λ_{max} (nm)
citrate (np-Au-cit)	-18.8 +/- 0.4	518
6-amino-1-hexanethiol hydrochloride (np-Au-NH_2)	31.9 +/- 7.3	525
6-amino-1-hexanethiol hydrochloride/ MUTEG (np-Au-NH_2/MUTEG)	21.2 +/- 3.2	550
MUTEG (np-MUTEG)	44.8 +/- 0.7	521

[1]All particles are synthesized from the same citrate stabilized core (17.0 +/- 1.6 nm as measured by TEM, n=61)

After crystallization in the presence of np-Au-NH_2, sparse interaction between gold nanoparticles and cuprite crystals was observed in SEM (Fig. 3a). Gold nanoparticles were also observed on the surface of the slide. Based upon the sparse coverage of the cuprite crystals, there is no evidence for any preferential interaction between the crystals and the amine-functionalized gold particles.

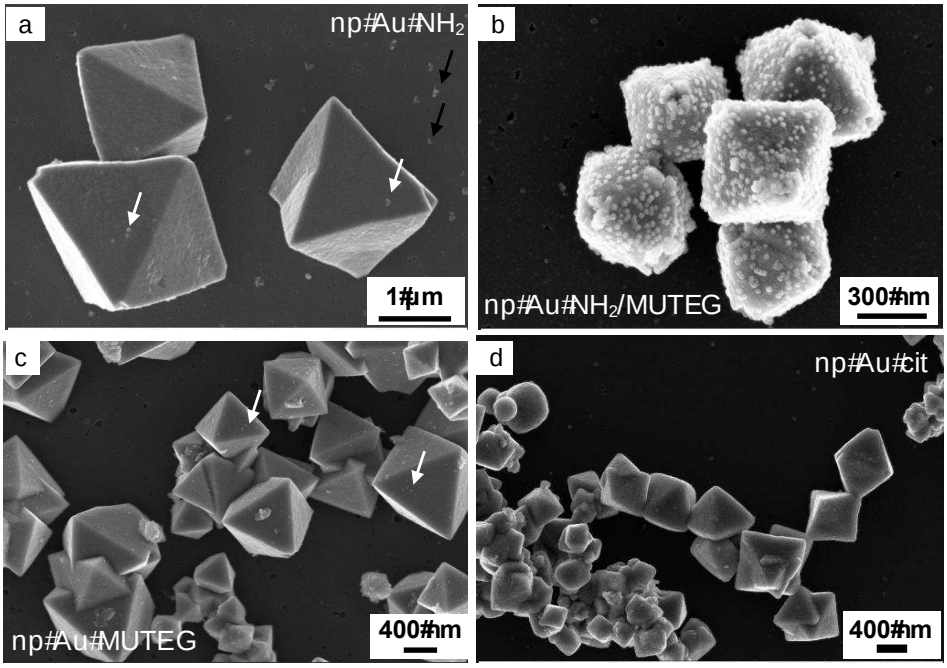

Figure 3. Change in crystal morphology and interaction with gold nanoparticles as a result of surface functionalization of gold nanoparticles in the wedge with silanization. All SEM images are taken from region A of the substrate. (a) Cu_2O and np-Au-NH_2. No significant interaction is observed; few particles appear on the surface of the crystals, as indicated by the white arrows. Interaction of the particles is also observed with the glass slide, as indicated by black arrows. (b) Cu_2O and np-Au-NH_2/MUTEG. A different morphology is observed and gold nanoparticles decorate the surface of the Cu_2O. (c) Cu_2O and np-Au-MUTEG. No significant interaction is observed; few particles appear on the surface of the crystals, as indicated by the white arrows. (d) Cu_2O and np-Au-cit. No significant interaction between the particles and the crystals is observed, and the octahedral morphology is less regular.

In order to strengthen the interaction of gold nanoparticles and Cu_2O crystals, we sought to further stabilize the particles in a manner consistent with past experiments. Hydrophilic but uncharged ligands such as oligo(ethylene glycol) are often mixed with charged ligands to improve the dispersability of nanoparticles in water.[49] Similarly, diblock copolymers consisting of a strong acid block and an electrosteric stabilizer block have been used as surface functionalization for magnetite nanoparticles, enabling the uniform incorporation of these particles in calcite single crystals.[16,17] With these experiments in mind, we selected (1-mercaptoundec-11-yl)tetra(ethylene glycol) (MUTEG) as a stabilizer for our system. Through

functionalizing gold nanoparticles with a balance of interacting and non-interacting components (6-amino-1-hexanethiol hydrochloride and MUTEG, respectively), the surface charge of the particles was successfully reduced, resulting in mixed-functionality np-Au-NH_2/MUTEG with a zeta potential of 21.2 +/- 3.2 mV (Table 1).

In contrast to the np-Au-NH_2, the np-Au-NH_2/MUTEG were seen to heavily decorate the entire surface of the cuprite crystals found in region A of the substrate, with optimized interaction observed at approximately 0.07 cm spacing between the top and bottom slides of the wedge (Fig. 3b and 4e,f; for regions B and C refer to Fig. S3). A slight morphological change was also observed; more octahedra were present in the system with both substrate and particle functionalization than with either element in isolation. As controls, np-Au-MUTEG and np-Au-cit did not display as much interaction with the cuprite octahedra (Fig. 3c,d; Fig. S4). Based upon the SEM images, the mixed-functionality gold nanoparticles appeared to be covered by an overgrowth of cuprite, suggesting more than just a superficial surface decoration. After cracking the crystals open with a pestle, SEM analysis revealed that particles were embedded near the crystal surface; however, they did not penetrate throughout the interior of the crystal (Fig. S5a). TEM analysis revealed that a thin (approximately 5 nm) layer of Cu_2O covers the gold nanoparticles (Fig. S5b).

Control experiments with the np-Au-NH_2/MUTEG in solution were performed to evaluate the effect of physical confinement on this system. A loss of control over morphology was observed (Fig. 4a,b for SEM; Fig. S1b for pXRD,). Some Cu_2O crystals had np-Au-NH_2/MUTEG associated with them, but such interactions were neither present across all morphologies, nor were consistent within a single morphology, such as octahedra (Fig. 4b). This trend was confirmed through an additional control experiment in which a silanized slide was completely covered in crystallization solution containing np-Au-NH_2/MUTEG (Fig. 4c,d). In this experiment, while most Cu_2O crystals had a small number of np-Au-NH_2/MUTEG on their surfaces, the coverage was not as great as that observed within the closed wedge. It is therefore evident that

the confinement of the wedge structure controls the morphology and monodispersity of the Cu_2O, as well as the interaction between the crystals and Au nps.

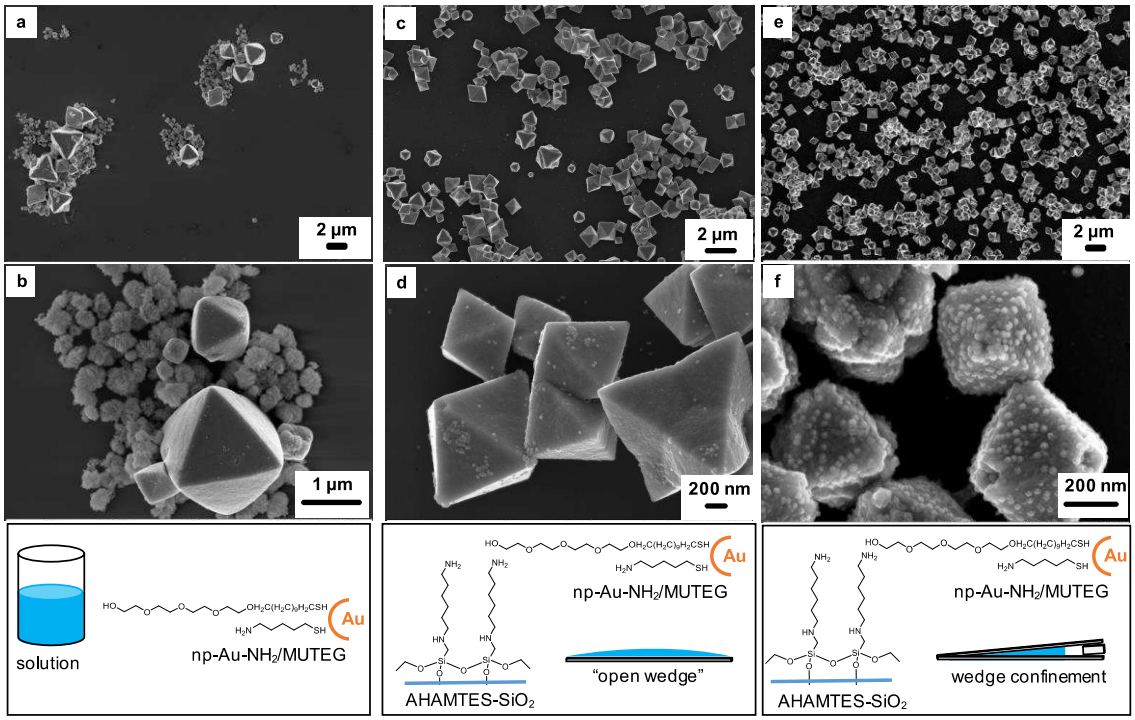

Figure 4. SEM images at low (a,c,e) and high (b,d,f) magnification in a,b) bulk solution with np-Au-NH_2/MUTEG, demonstrating a loss of uniform morphology and little interaction of the Au np with the cuprite crystals; c,d) a silanized slide with np-Au-NH_2/MUTEG, demonstrating the role of the silanized surface in promoting uniform particle morphologies, but a lack of interaction with the particles in the absence of confinement; and e,f) a silanized wedge with np-Au-NH_2/MUTEG, demonstrating crystallization with both physical and chemical control. Uniformity of octahedral morphology, coverage of the substrate, and association of the Au nps with the cuprite crystals are all optimized with confinement and added chemical functionality.

Finally, a series of experiments was performed to determine the degree of surface functionalization necessary to promote the interaction between Cu_2O and gold nanoparticles. The morphologies of Cu_2O grown with np-Au-cit in a piranha-cleaned, native-oxide wedge (Fig. S6) and with np-Au-cit in a silanized wedge (Fig. 3d and S4) were compared with the optimized conditions of np-Au-NH_2/MUTEG in a silanized wedge (Fig. 4e,f). Better coverage of the substrate and a higher proportion of octahedra were achieved with both functionalized particles

and silanization than with one element alone, although the diffusion gradient itself (Figs. 2, S3) remained unchanged with particle functionality or substrate functionality. These experiments demonstrate the ability of optimized chemical functionality (on both the gold nanoparticles and the substrate) in concert with the physical control of the wedge structure to increase the interaction between gold nanoparticles and Cu_2O.

Discussion

In this work, we examined the complex interplay amongst three key design features for promoting the growth of cuprite-Au heterostructures: 1) The "reactor" wedge geometry; 2) the chemical functionalization of the glass slides used to form the wedge; and 3) the surface functionality on the gold nanoparticles. We optimized the synthetic process to obtain a high yield of cuprite octahedra expressing {111} facets. These octahedra are heavily decorated with gold nanoparticles encapsulated within a thin overlayer of cuprite, which encapsulated the Au nps (Figs. 3c, 4e,f). To achieve this desired heterostructure, we crystallized the cuprite in the presence of NH_2/MUTEG-Au-np within a wedge formed from amine-terminated, silanized glass slides. Through a series of carefully designed experiments, we identified key features responsible for the observed results.

It is helpful to categorize the multiple variables into physical and chemical features. The wedge geometry was used to exert physical control over the crystallization microenvironment. In the central images in Figs. 2 and S3, the presence of macroscopic gradients formed in the wedge are obvious. Further examination by SEM reveals that the different regions have characteristic crystal morphologies, while pXRD reveals that only the cuprite phase is present. The spatial variation in color and crystal morphology most likely results from diffusion gradients of the hydrazine vapor leading to different nucleation and growth rates in each region. The "sweet spot" for octahedra expressing {111} facets is near the edges in the middle 1/3 of the slide. This morphology is desirable because the close-packed {111} facets are associated with increased electrical performance of these materials.[50] Towards the interior of the slide and near

the closed end of the wedge, highly irregular morphologies form and coverage is poor. Similar spatial variations in crystal morphology within a wedge have been reported for calcite[18] and are consistent with growth-rate dependent morphology changes.[51]

Chemical functionalization of the glass slides by silanization with an amine-terminated silane improved the adhesion of the cuprite crystals and therefore silanized slides were used in all experiments. The affinity of Cu^{2+} for strong-field amine ligands is well-established in the inorganic chemistry literature,[52] and is most likely responsible for the observed attraction between the cuprite crystals and amine-functionalized substrates.[11] It is important to note that the observed gradients, and the crystal morphologies do not change significantly as a function of silanization (compare Fig. 2 and S3), which emphasizes that it is the solution chemistry (reagent concentrations, etc.) that controls the morphology, rather than the surface chemistry.

Upon addition of gold nanoparticles to the wedge setup, several key observations are made concerning both the chemical and physical features of the system:

1) The surface functionalization of the Au np plays an essential role in determining the extent of interaction with the cuprite crystals. Only the Au nps with mixed functionality, NH_2/MUTEG show heavy coverage of the cuprite crystals. As already discussed, the Cu^{2+}-amine affinity is well-known; however, nanoparticles with only amine-terminated thiols do not bind strongly to the cuprite crystals. Upon dilution with the steric stabilizer MUTEG, the particle behavior changes dramatically, and heavy coverage of the cuprite crystals is observed. This result suggests that there is an optimum surface charge and ligand density that promotes strong association with the mineral surface, consistent with recent reports of polymeric micelles and calcite.[16,17,53]
2) The confining geometry of the wedge is also necessary to drive the association of the Au nps with the growing cuprite crystals. In either bulk solution or on a silanized slide, cuprite crystals grown with NH_2/MUTEG particles do not display the same degree of surface coverage as those grown in the wedge (Fig. 4a-d). In bulk solution a range of

crystal morphologies are observed, reemphasizing the control over crystal growth kinetics afforded by the confines of the wedge geometry. The introduction of a silanized slide does increase the uniformity of crystal morphologies, as is consistent with literature reports. However, in neither of these control experiments, which probe the importance of the wedge geometry, do we observe significant coverage of the cuprite crystals with the NH_2/MUTEG Au nps. This key observation points to an additional role of the confining wedge geometry in limiting the diffusion of the Au nps, suppressing convective currents, and/or driving the particles towards the crystals. Related reports have demonstrated the use of gel networks to immobilize inorganic nanoparticles, thus facilitating their incorporation into calcite crystals.[54,55] Clearly the mobility of the "guest phase" is an important variable for determining interaction between the crystal and nanoparticles. The current work provides another demonstration of this phenomenon and establishes the wedge geometry as a general approach for achieving this effect.

3) Only a thin layer of Cu_2O grows over the Au nps, rather than achieving full incorporation throughout the bulk of the crystals. Similar surface layer incorporation has been reported for other particle-crystal systems and is usually attributed to a competition between growth rate and strength of attraction between the two components.[56,57] In the current system, we propose that a combination of the limited supply of Cu^{2+} ions (as a result of small reaction volumes) and the vapor diffusion of hydrazine is responsible for controlling the growth rate of the crystallization. Similarly, we hypothesize that the limited volume allows for only a thin layer of Cu_2O to grow over the embedded nanoparticles before eventual frustration of growth as a result of depletion of free ions.

This work demonstrates that physical confinement, combined with chemical control imparted by the local surface chemistry of the template and the surface functionality of nanoparticles, has the potential to control the interaction of guest species with a selected host crystal. Based upon literature examples of a range of other crystals grown within

confinement[32,36,58,59] coupled with the growing number of examples of small organic molecules and functionalized particles able to incorporate into crystalline oxides,[60-62] we anticipate that the strategy presented here will be widely applicable to a range of host crystal – particle guest pairs.

Conclusions

Through confinement-limited diffusion (a physical parameter), and surface functionalization (a chemical parameter), we have achieved control over the interaction of Au nanoparticles and Cu_2O during crystallization, leading to the formation of metal-semiconductor heterostructures. Using physical confinement alone, morphology of the cuprite crystals is controlled but no interaction is observed between Au np and Cu_2O. By contrast, with only functionalized Au np in bulk solution, poor morphological control is observed in the Cu_2O. It is only with both confinement and surface functionalization that control over the interaction between gold nanoparticles and Cu_2O is achieved. Given the ability of confinement in concert with surface functionalization to encourage interaction between gold nanoparticles and Cu_2O, with optimization this design strategy has the potential to direct the formation of other metal-semiconductor heterostructures for a wide range of optoelectronic applications.

Acknowledgments

We acknowledge support from the NSF Materials World Network Program (DMR 1210304, LAE). AED acknowledges funding from the Cornell University College of Arts and Sciences through the Einhorn Discovery Grant and the Cornell Abroad and Undergraduate Research Funding Programs. EAS acknowledges the NSF Graduate Research Fellowship (GRF, DGE-0707428), and Integrative Graduate Education and Research Traineeship (IGERT, DGE-0903653) Programs. This work was also supported in part by The Cornell Center for Materials Research (CCMR) and made use of the CCMR Shared Facilities, both funded by NSF MRSEC program (DMR 1120296). We also acknowledge support from an Engineering and

Physical Sciences Research Council (EPSRC) Materials World Network grant (EP/J018589/1, FCM) and EPSRC grant EP/K006304/1 (FCM and ANK). This work made use of the Nanobiotechnology Center for Shared Research at Cornell University.

Supporting Information

Figures S1-S6: pXRD plots and supplemental SEM and TEM images are included in supporting information. This material is available free of charge via the internet at http://pubs.acs.org.

REFERENCES

(1) Jiang, R.; Li, B.; Fang, C.; Wang, J. Adv. Mater. **2014**, 26, 5274.

(2) Costi, R.; Saunders, A. E.; Banin, U. Angew. Chem. Int. Ed. **2010**, 49, 4878.

(3) Wei, J.; Jiang, N.; Xu, J.; Bai, X.; Liu, J. Nano Lett. **2015**, 15, 5926.

(4) Cushing, S. K.; Li, J. T.; Meng, F. K.; Senty, T. R.; Suri, S.; Zhi, M. J.; Li, M.; Bristow, A. D.; Wu, N. Q. J. Am. Chem. Soc. **2012**, 134, 15033.

(5) Wang, X.; Peng, K. Q.; Hu, Y.; Zhang, F. Q.; Hu, B.; Li, L.; Wang, M.; Meng, X. M.; Lee, S. T. Nano Lett. **2014**, 14, 18.

(6) Zhang, L.; Blom, D. A.; Wang, H. Chem. Mater. **2011**, 23, 4587.

(7) Pan, Y. L.; Deng, S. Z.; Polavarapu, L.; Gao, N. Y.; Yuan, P. Y.; Sow, C. H.; Xu, Q. H. Langmuir **2012**, 28, 12304.

(8) Lin, Y. K.; Chiang, Y. J.; Hsu, Y. J. Sensors and Actuators B-Chemical **2014**, 204, 190.

(9) Rai, P.; Khan, R.; Raj, S.; Majhi, S. M.; Park, K. K.; Yu, Y. T.; Lee, I. H.; Sekhar, P. K. Nanoscale **2014**, 6, 581.

(10) Nepal, D.; Drummy, L. F.; Biswas, S.; Park, K.; Vaia, R. A. ACS Nano **2013**, 7, 9064.

(11) Susman, M. D.; Feldman, Y.; Vaskevich, A.; Rubinstein, I. ACS Nano **2014**, 8, 162.

(12) Kim, Y.-Y.; Ganesan, K.; Yang, P.; Kulak, A. N.; Borukhin, S.; Pechook, S.; Ribeiro, L.; Kröger, R.; Eichhorn, S. J.; Armes, S. P.; Pokroy, B.; Meldrum, F. C. Nat Mater **2011**, 10, 890.

(13) Li, H. Y.; Xin, H. L.; Muller, D. A.; Estroff, L. A. Science **2009**, 326, 1244.

(14) Li, H.; Xin, H. L.; Kunitake, M. E.; Keene, E. C.; Muller, D. A.; Estroff, L. A. Adv. Funct. Mater. **2011**, 21, 2028.

(15) Kim, Y.-Y.; Semsarilar, M.; Carloni, J. D.; Cho, K. R.; Kulak, A. N.; Polishchuk, I.; Hendley, C. T.; Smeets, P. J. M.; Fielding, L. A.; Pokroy, B.; Tang, C. C.; Estroff, L. A.; Baker, S. P.; Armes, S. P.; Meldrum, F. C. Adv. Funct. Mater. **2016**, 26, 1382.

(16) Kulak, A. N.; Semsarilar, M.; Kim, Y. Y.; Ihli, J.; Fielding, L. A.; Cespedes, O.; Armes, S. P.; Meldrum, F. C. Chemical Science **2014**, 5, 738.

(17) Kulak, A. N.; Yang, P. C.; Kim, Y. Y.; Armes, S. P.; Meldrum, F. C. Chem. Commun. **2014**, 50, 67.

(18) Hetherington, N. B. J.; Kulak, A. N.; Kim, Y. Y.; Noel, E. H.; Snoswell, D.; Butler, M.; Meldrum, F. C. Adv. Funct. Mater. **2011**, 21, 948.

(19) Lu, C. H.; Qi, L. M.; Cong, H. L.; Wang, X. Y.; Yang, J. H.; Yang, L. L.; Zhang, D. Y.; Ma, J. M.; Cao, W. X. Chem. Mater. **2005**, 17, 5218.

(20) Munoz-Espi, R.; Chandra, A.; Wegner, G. Crystal Growth Des. **2006**, 1584.

(21) Cho, K.-R.; Kim, Y.-Y.; Yang, P.; Cai, W.; Pan, H.; Kulak, A. N.; Lau, J. L.; Kulshreshtha, P.; Armes, S. P.; Meldrum, F. C.; De Yoreo, J. J. Nat Commun **2016**, 7.

(22) Sear, R. P. CrystEngComm **2014**, 16, 6506.

(23) Ihli, J.; Bots, P.; Kulak, A.; Benning, L. G.; Meldrum, F. C. Adv. Funct. Mater. **2013**, 23, 1965.

(24) Rycenga, M.; Camargo, P. H. C.; Xia, Y. N. Soft Matter **2009**, 5, 1129.

(25) Loste, E.; Park, R. J.; Warren, J.; Meldrum, F. C. Adv. Funct. Mater. **2004**, 14, 1211.

(26) Cantaert, B.; Beniash, E.; Meldrum, F. C. Chem. Eur. J. **2013**, 19, 14918.

(27) Stephens, C. J.; Ladden, S. F.; Meldrum, F. C.; Christenson, H. K. Adv. Funct. Mater. **2010**, 20, 2108.

(28) Wang, Y.-W.; Christenson, H. K.; Meldrum, F. C. Adv. Funct. Mater. **2013**, 23, 5615.

(29) Hamilton, B. D.; Hillmyer, M. A.; Ward, M. D. Cryst. Growth Des. **2008**, 8, 3368.

(30) Ha, J. M.; Wolf, J. H.; Hillmyer, M. A.; Ward, M. D. J. Am. Chem. Soc. **2004**, 126, 3382.

(31) Mann, S.; Hannington, J. P.; Williams, R. J. P. Nature **1986**, 324, 565.

(32) Tester, C. C.; Whittaker, M. L.; Joester, D. Chem. Commun. **2014**, 50, 5619.

(33) Jasinska, B.; Dawidowicz, A. L.; Pikus, S. Acta Physica Polonica A **2005**, 107, 724.

(34) Gong, X.; Wang, Y.-W.; Ihli, J.; Kim, Y.-Y.; Li, S.; Walshaw, R.; Chen, L.; Meldrum, F. C. Adv. Mater. **2015**, 27, 7395.

(35) Jiang, Q.; Ward, M. D. Chem. Soc. Rev. **2014**, 43, 2066.

(36) Whittaker, M. L.; Dove, P. M.; Joester, D. MRS Bull. **2016**, 41, 388.

(37) Polman, A.; Atwater, H. A. Nat Mater **2012**, 11, 174.

(38) Li, X.; Jiang, Y.; Shi, Z. W.; Xu, Z. Chem. Mater. **2007**, 19, 5424.

(39) Li, X.; Tao, F.; Jiang, Y.; Xu, Z. J. Colloid Interface Sci. **2007**, 308, 460.

(40) Ivanov, M. R.; Bednar, H. R.; Haes, A. J. ACS Nano **2009**, 3, 386.

(41) Kowalczyk, B.; Bishop, K. J. M.; Lagzi, I.; Wang, D. W.; Wei, Y. H.; Han, S. B.; Grzybowski, B. A. Nature Mater. **2012**, 11, 227.

(42) Love, J. C.; Estroff, L. A.; Kriebel, J. K.; Nuzzo, R. G.; Whitesides, G. M. Chem. Rev. **2005**, 105, 1103.

(43) Kimling, J.; Maier, M.; Okenve, B.; Kotaidis, V.; Ballot, H.; Plech, A. J. Phys. Chem. B **2006**, 110, 15700.

(44) Haiss, W.; Thanh, N. T. K.; Aveyard, J.; Fernig, D. G. Anal. Chem. **2007**, 79, 4215.

(45) Asenath-Smith, E.; Chen, W. Langmuir **2008**, 24, 12405.

(46) Benedict, S. R. J. Biol. Chem. **1909**, 5, 485.

(47) Susman, M. D.; Feldman, Y.; Vaskevich, A.; Rubinstein, I. Chem. Mater. **2012**, 24, 2501.

(48) Turkevich, J.; Stevenson, P. C.; Hillier, J. Discussions of the Faraday Society **1951**, 55.

(49) You, C. C.; Verma, A.; Rotello, V. M. Soft Matter **2006**, 2, 190.

(50) Kuo, C. H.; Yang, Y. C.; Gwo, S.; Huang, M. H. J. Am. Chem. Soc. **2011**, 133, 1052.

(51) Chernov, A. A. Modern Crystallography III: Crystal Growth; Springer-Verlag: New York, 1984; Vol. 36.

(52) Cotton, F. A. Advanced Inorganic Chemistry; 6 ed.; Wiley-Interscience: New York, 1999.

(53) Ning, Y.; Fielding, L. A.; Ratcliffe, L. P. D.; Wang, Y. W.; Meldrum, F. C.; Armes, S. P. J. Am. Chem. Soc. **2016**, 138, 11734.

(54) Liu, Y.; Yuan, W.; Shi, Y.; Chen, X.; Wang, Y.; Chen, H.; Li, H. Angew. Chem. Int. Ed. **2014**, 53, 4127.

(55) Liu, Y.; Zang, J.; Wang, L.; Fu, W.; Yuan, W.; Wu, J.; Jin, X.; Han, J.; Wu, C. H.; Wang, Y.; Xin, H. L.; Chen, H.; Li, H. Chem. Mater. **2016**.

(56) Kim, Y. Y.; Ribeiro, L.; Maillot, F.; Ward, O.; Eichhorn, S. J.; Meldrum, F. C. Adv. Mater. **2010**, 22, 2082.

(57) Munoz-Espi, R.; Qi, Y.; Lieberwirth, I.; Gomez, C. M.; Wegner, G. Chem. Eur. J. **2006**, 12, 118.

(58) Wang, Y. W.; Christenson, H. K.; Meldrum, F. C. Adv. Funct. Mater. **2013**, 23, 5615.

(59) Anduix-Canto, C.; Kim, Y. Y.; Wang, Y. W.; Kulak, A.; Meldrum, F. C.; Christenson, H. K. Cryst. Growth Des. **2016**, 16, 5403.

(60) Weber, E.; Pokroy, B. CrystEngComm **2015**, 17, 5873.

(61) Brif, A.; Ankonina, G.; Drathen, C.; Pokroy, B. Adv. Mater. **2014**, 26, 477.

(62) Kulak, A. N.; Grimes, R.; Kim, Y.-Y.; Semsarilar, M.; Anduix-Canto, C.; Cespedes, O.; Armes, S. P.; Meldrum, F. C. Chem. Mater. **2016**, acs.chemmater.6b03563.

For Table of Contents Use Only

Title:
Cooperative Effects of Confinement and Surface Functionalization Enable the Formation of Au/Cu_2O Metal-Semiconductor Heterostructures

Authors:
Allessandra E. DiCorato, Emily Asenath-Smith, Alex N. Kulak, Fiona C. Meldrum, and Lara A. Estroff

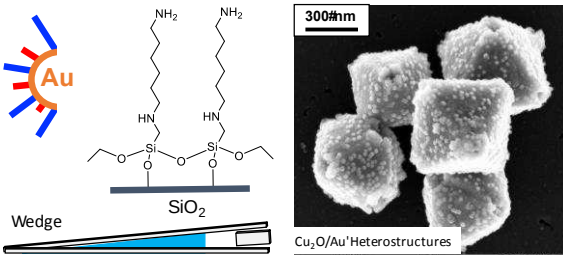

Synopsis: Crystallization in confinement of copper (I) oxide (Cu_2O) in the presence of alkanethiol-functionalized gold nanoparticles (Au nps) promotes the formation of a metal-semiconductor heterostructure. Both the physical confinement of the wedge structure as well as chemical functionalization of the glass slides and the Au np surfaces are required to achieve the incorporation of Au nps into the growing Cu_2O crystals.